NASA/TP–2013-217983

Radiation Shielding Optimization on Mars

Tony C. Slaba, Christopher J. Mertens, and Steve R. Blattnig
Langley Research Center, Hampton, Virginia

April 2013

NASA STI Program . . . in Profile

Since its founding, NASA has been dedicated to the advancement of aeronautics and space science. The NASA scientific and technical information (STI) program plays a key part in helping NASA maintain this important role.

The NASA STI program operates under the auspices of the Agency Chief Information Officer. It collects, organizes, provides for archiving, and disseminates NASA's STI. The NASA STI program provides access to the NASA Aeronautics and Space Database and its public interface, the NASA Technical Report Server, thus providing one of the largest collections of aeronautical and space science STI in the world. Results are published in both non-NASA channels and by NASA in the NASA STI Report Series, which includes the following report types:

- TECHNICAL PUBLICATION. Reports of completed research or a major significant phase of research that present the results of NASA Programs and include extensive data or theoretical analysis. Includes compilations of significant scientific and technical data and information deemed to be of continuing reference value. NASA counterpart of peer-reviewed formal professional papers, but having less stringent limitations on manuscript length and extent of graphic presentations.

- TECHNICAL MEMORANDUM. Scientific and technical findings that are preliminary or of specialized interest, e.g., quick release reports, working papers, and bibliographies that contain minimal annotation. Does not contain extensive analysis.

- CONTRACTOR REPORT. Scientific and technical findings by NASA-sponsored contractors and grantees.

- CONFERENCE PUBLICATION. Collected papers from scientific and technical conferences, symposia, seminars, or other meetings sponsored or co-sponsored by NASA.

- SPECIAL PUBLICATION. Scientific, technical, or historical information from NASA programs, projects, and missions, often concerned with subjects having substantial public interest.

- TECHNICAL TRANSLATION. English-language translations of foreign scientific and technical material pertinent to NASA's mission.

Specialized services also include organizing and publishing research results, distributing specialized research announcements and feeds, providing information desk and personal search support, and enabling data exchange services.

For more information about the NASA STI program, see the following:

- Access the NASA STI program home page at *http://www.sti.nasa.gov*

- E-mail your question to help@sti.nasa.gov

- Fax your question to the NASA STI Information Desk at 443-757-5803

- Phone the NASA STI Information Desk at 443-757-5802

- Write to:
  STI Information Desk
  NASA Center for AeroSpace Information
  7115 Standard Drive
  Hanover, MD 21076-1320

NASA/TP–2013-217983

Radiation Shielding Optimization on Mars

Tony C. Slaba, Christopher J. Mertens, and Steve R. Blattnig
Langley Research Center, Hampton, Virginia

National Aeronautics and
Space Administration

Langley Research Center
Hampton, Virginia 23681-2199

April 2013

Available from:

NASA Center for AeroSpace Information
7115 Standard Drive
Hanover, MD 21076-1320
443-757-5802

Contents

Figures

Tables

Abstract

Future space missions to Mars will require radiation shielding to be optimized for deep space transit and an extended stay on the surface. In deep space, increased shielding levels and material optimization will reduce the exposure from most solar particle events (SPE) but are less effective at shielding against galactic cosmic rays (GCR). On the surface, the shielding provided by the Martian atmosphere greatly reduces the exposure from most SPE, and long-term GCR exposure is a primary concern. Previous work has shown that in deep space, additional shielding of common materials such as aluminum or polyethylene does not significantly reduce the GCR exposure. In this work, it is shown that on the Martian surface, almost any amount of aluminum shielding increases exposure levels for humans. The increased exposure levels are attributed to neutron production in the shield and Martian regolith as well as the electromagnetic cascade induced in the Martian atmosphere. This result is significant for optimization of vehicle and shield designs intended for the surface of Mars.

1. Introduction

Future missions to Mars will include a relatively long duration transit time in deep space as well as an extended stay on the surface. Possible mission durations are likely to range from 500-1000 days with surface stays ranging from 30-500 days [NASA 2009]. The transit will include continuous exposure from Galactic Cosmic Rays (GCR) as well as the possibility for one or more Solar Particle Events (SPE). Vehicle design and material optimization in deep space radiation environments has been studied extensively [Cucinotta et al. 2012, Wilson et al. 1997, 2004], and it has been found that exposure from SPE can be effectively mitigated with appropriate shielding materials and thicknesses. However, exposure from GCR is only moderately reduced by shield optimization, and exposure levels can actually be slightly amplified within a vehicle due to neutron build-up if shielding thicknesses exceed 50 g/cm^2 for certain materials such as aluminum.

The radiation environment on the Martian surface is characteristically different than in deep space. SPE are greatly attenuated as they pass through the atmosphere, and the exposure level on the surface is reduced by approximately an order of magnitude. The exposure from GCR is somewhat reduced in passing through the atmosphere; however, interactions between incoming ions and the atmospheric constituents result in pion production and an electromagnetic cascade that contributes to exposure on the surface. There are also nuclear collisions between GCR ions and the Martian soil creating an ambient field of neutrons that contribute to the total exposure. Other secondary reaction products are also present on the surface, but their contribution to total exposure and biological risk is small [Dartnell et al. 2007a].

For radiation shield optimization on the Martian surface, exposure levels need to be provided for a range of shielding thicknesses and materials and should include albedo neutrons as well as the pion-electromagnetic (π/EM) cascade induced in the atmosphere. Exposure levels and mitigation strategies for the Martian surface have been examined in the past [Cucinotta et al. 2010, Saganti et al. 2004, Zeitlin et al. 2004, Kim et al. 1998, Simonsen and Nealy 1991], and most of these studies utilized the radiation transport code, HZETRN (High charge (Z) and Energy TRaNsport), within the straight-ahead approximation [Wilson et al. 1991, 2006]. In this radiation transport model, all particles are assumed to propagate along a common axis, and the contribution from backscattered neutrons is not included. The contribution from π/EM interactions is also not included. Clowdsley et al. [2000] did include a model for backward moving neutrons into HZETRN and estimated the neutron energy spectrum on the Martian surface; however, no detailed shielding studies were included. Monte Carlo analyses have also been performed [McKenna-Lawlor et al. 2012a, 2012b; Borggrafe et al. 2009; Dartnell et al. 2007a, 2007b; Morthekai et al. 2007], but results have only been provided for no shielding or very specific shielding configurations.

Recent extensions to HZETRN have included an improved bi-directional neutron transport model that is fully coupled to light ion ($Z < 2$) target fragment production [Slaba et al. 2010a, 2011]. The model has been compared to three dimensional Monte Carlo codes for both slab geometries and lunar surface calculations and found to agree with the Monte Carlo codes to the extent they agree with each other. The π/EM transport model originally developed by Blattnig et al. [2004] was also recently integrated into

HZETRN [Norman et al. 2012, 2013] and compared to Monte Carlo codes [Slaba et al. 2013]. While improvements to the model are necessary, the initial comparisons clearly showed the importance of π/EM interactions in GCR transport calculations, and reasonable agreement was found between the codes at large shielding thicknesses. For transport through the Martian atmosphere, vertical atmospheric shielding ranges from 16-22 g/cm^2 [Simonsen and Nealy 1991], but off-axis rays closer to the horizon easily exceed 100 g/cm^2.

In this work, dose equivalent and effective dose results are presented as a function of aluminum and polyethylene spherical shielding thickness on the Martian surface. The contributions from back-scattered neutrons and the π/EM cascade are explicitly separated. It is shown that surface exposures increase with almost any amount of aluminum shielding. These findings are significant for vehicle design and material optimization on the Martian surface. This paper is organized as follows. In section 2, the computational tools used to compute exposure on the Martian surface are described. Results and discussion are given in section 3. Summary and conclusions are given in section 4.

2. Computational Models

Martian surface exposure

In Figure 1, a representative geometry that was used for the surface calculations is shown. In order to calculate dose equivalent or effective dose at the target point, the particle fluxes are needed. The fluxes are computed by using a ray-by-ray transport methodology with HZETRN including the π/EM and bi-directional neutron transport (HZETRN- π/EM) [Wilson et al. 1991; Slaba et al. 2010a, 2010b; Norman et al. 2013]. In this approach, a large number of rays are extended in all directions from the target point through the shield material and through either the atmosphere or regolith, depending on the ray-direction. The atmospheric thickness and density profile along any slant angle is determined from a vertical density profile through trigonometric relationships [Simonsen et al. 1990]. The vertical density profile provides atmospheric density as a function of elevation above the surface. The profile used in this study will be discussed later in this section. The regolith thickness traversed by any ray extending down into the surface is set to 300 g/cm^2. This approximates Mars as a large hemisphere under the spherical shield. Sensitivity studies were performed to ensure that 300 g/cm^2 is sufficiently thick to ensure equilibrium in the back-scattered neutron field. The atmospheric composition from De Angelis et al. [2004] and regolith composition from McKenna-Lawlor et al. [2012a] are used in the present work. The atmospheric composition is mainly CO_2 with a trace amount of argon. The regolith composition is a global average containing 51.2% SiO_2, 9.3% Fe_2O_3, and 7.4% H_2O with the remaining 32.1% comprised mainly of elements between oxygen and calcium. It should be noted that the small amount of water included in the composition corresponds to a hydrogen mass fraction of < 1%. The majority of the regolith composition is given by 47% oxygen and 24% silicon.

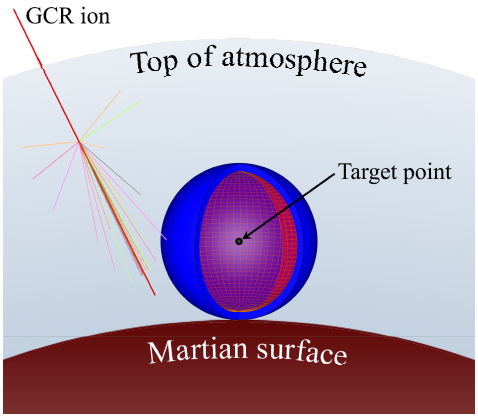

Figure 1. Representative geometry used for the surface calculations.

Radiation transport is performed separately on each ray that enters the top of the atmosphere, passes through the vehicle, and propagates into the surface. These rays will be referred to as "downward" pointing rays. The exposure along all other rays (i.e. rays entering from the regolith beneath the vehicle and extending into the atmosphere) is assumed to be zero, thereby accounting for the 2π blockage provided by the surface. The total flux at the target point is obtained by integrating the fluxes computed for each ray.

In order to compute effective dose, a human phantom model is placed in the sphere, and 1208 target points are distributed throughout the body in radiosensitive tissues [Slaba et al. 2010c]. Transport is performed along downward rays for each human target point separately. In this work, 968 rays were used for all calculations. It should be noted that whether or not the human is included, the ray-by-ray transport approach imposes no restriction on the number or order of materials along each ray. This is in contrast to interpolation-based methods using HZETRN that have been generally restricted to at most 3 or 4 layers and require strict ordering of materials. In this work, dose equivalent is calculated using the ICRP 60 quality factor [ICRP 1990], and for effective dose, the FAX (Female Adult voXel) human phantom [Kramer et al. 2004] is used with the ICRP 103 tissue weights [ICRP 2007]. Unless specified otherwise, the free space GCR environment is described by the Badhwar-O'Neill 2010 (BON2010) model [O'Neill 2010] using a solar modulation parameter of 475 MV to represent solar minimum conditions.

Atmospheric density profile

The vertical density profile used in this work to derive slant angle atmospheric thicknesses and density profiles is computed with the Mars Climate Database (MCD) model [Millour et al. 2008]. The MCD model is a meteorological database derived from numerical simulations and validated against available measurements. As inputs into the MCD model, the approximate landing time and location of the Curiosity rover were used. Curiosity landed on August 6, 2012 corresponding to a Martian solar longitude of L_s = 150.6°, and the coordinates of the landing site in Gale Crater were set to -4.6° N, 137.4° E. In the right pane of Figure 2, total atmospheric thickness (g/cm^2) is plotted as a function of inclination angle. For inclination angles greater than ~45°, the cumulative atmospheric thickness ranges from 20-30 g/cm^2. However, it is clear that lower inclination rays have much larger thicknesses that can exceed 100 g/cm^2.

In the left pane of Figure 2, the cumulative atmospheric thickness is plotted as a function of atmospheric density. The density changes by over 4 orders of magnitude between the top of the atmosphere and the surface. Previous versions of HZETRN do not include decay processes, and only the total thickness along each ray was required for transport procedures. However, the charged pion and muon transport and EM cascade depends on the density of the medium. Consequently, the variation of density with atmospheric thickness along each ray is included in the transport procedure so that decay lengths are properly computed.

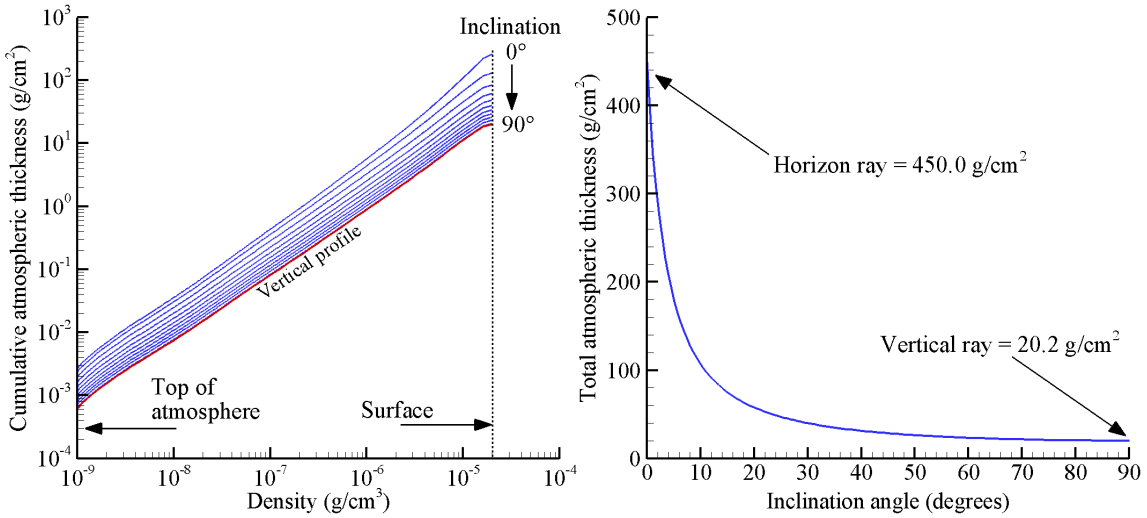

Figure 2. Cumulative atmospheric thickness for several inclination angles is plotted as a function of density (g/cm^3) in the left pane. Total atmospheric thickness (g/cm^2) is plotted as a function of inclination angle in the right pane.

3. Results

Comparison to Monte Carlo

In this section, the computational models described in section 2 are compared to published Monte Carlo results. McKenna-Lawlor et al. [2012b] used the Geant4 application, MEREM (Mars Energetic Radiation Environment Model), to compute the unshielded dose equivalent rate during solar minimum and solar maximum conditions on the Martian surface near the Viking 1 landing site. The atmospheric profile was retrieved from measured data but was not provided in the paper. The regolith composition was provided in a related paper [McKenna-Lawlor et al. 2012a]. The GCR environment was computed with the ISO (International Organization for Standardization) model based on the work of Nymmik et al. [1996]. December 2006 was used for the solar minimum period, and April 2002 was used for the solar maximum period.

In the current work, the atmospheric profile was computed with the MCD model described in section 2 using the Viking 1 landing site coordinates (L_s = 97°, 22.48° N, -49.97° E). The regolith composition provided by [McKenna-Lawlor et al. 2012a] was used directly. A plot of the GCR particle spectra was not provided in the paper; therefore, in the present work, results are generated with three different GCR models and compared. The BON2010 model, the model of Matthia et al. [2013], and the ISO model evaluated through the SPENVIS (SPace ENVironment Information System) [SPENVIS] website have been used. The BON2010 has been commonly used in space radiation analysis, and the Matthia model is derived from the ISO model.

Results are given in Table 1. The current computational model is within 20% of the detailed Monte Carlo calculation. Differences can be attributed to GCR and transport model differences and to a lesser extent, differences in the atmospheric density profile.

Table 1. Comparison of present calculations to results generated with the Geant4-based application, MEREM [McKenna-Lawlor et al. 2012b]. Dose equivalent values are in mSv/year and values in parentheses are the relative percent difference between present calculations and MEREM results.

	MEREM	Present ISO	Present Matthia	Present BON2010
Solar minimum	273.8	252.5 (-8%)	245.8 (-10%)	224.5 (-18%)
Solar maximum	156.4	183.0 (17%)	165.9 (6%)	155.3 (-1%)

Shielding Analysis

In Figure 3, dose equivalent (left pane) and effective dose (right pane) are plotted as a function of aluminum and polyethylene shield thickness. The total dose equivalent and effective dose values exhibit similar, but not identical, trends for aluminum and polyethylene. In particular, the dose equivalent values monotonically increase with aluminum thickness by 63% from 0 g/cm^2 to 100 g/cm^2. The effective dose values also initially increase with aluminum thickness but reach a maximum value around 60 g/cm^2. The total variation in effective dose values as a function of aluminum thickness is only 3%. For polyethylene, dose equivalent values are reduced by more than a factor of 2, and effective dose values are reduced by as much as 35%. For both materials, the variation in effective dose versus depth is smaller than the variation in dose equivalent versus depth. This is a result of secondary particle attenuation within tissue, particularly for neutrons. The effect is less pronounced in polyethylene because it moderates neutron production more effectively than aluminum.

There is a clear difference in the albedo neutron contribution to dose equivalent between aluminum and polyethylene. The decrease in albedo neutron contribution with polyethylene depth is a result of elastic collisions with hydrogen nuclei. The increase in albedo neutron contribution with aluminum depth is a result of inelastic collisions between neutrons and ions with target nuclei. The difference between the two materials is greatly reduced if effective dose values are considered. This is a result of elastic collisions with hydrogen nuclei occurring within tissue. The contribution from π/EM

interactions appears to be similar for both materials, with consistently smaller values observed in polyethylene. The reduction in polyethylene is attributed to reduced neutron production and neutron attenuation associated with elastic collisions as already noted. The difference between the two materials is at most 31% for dose equivalent and 13% for effective dose. It is also important to notice that for effective dose, the π/EM contribution is actually greater than the albedo neutron contribution for both materials across all depths.

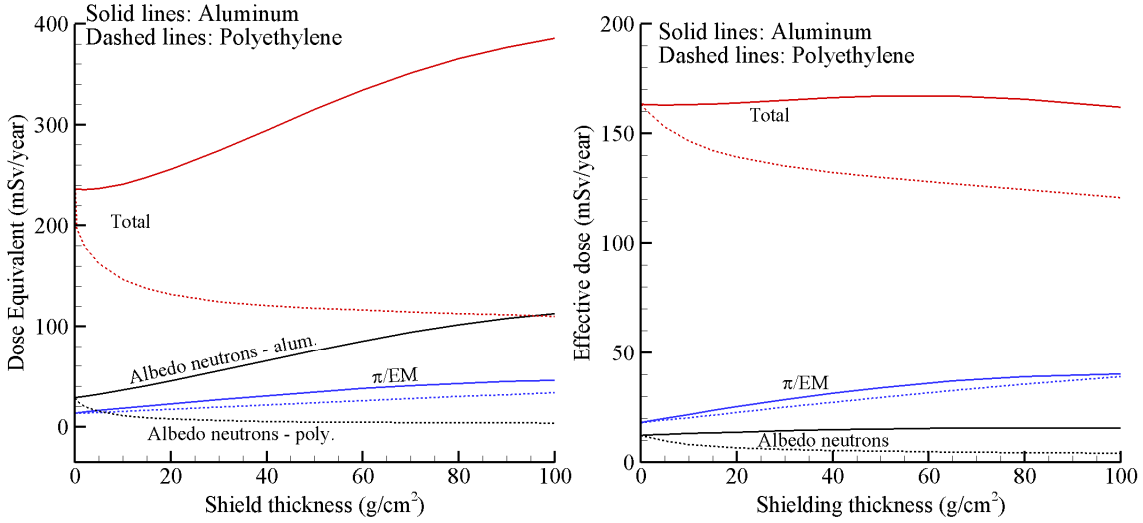

Figure 3. Dose equivalent (left pane) and effective dose (right pane) as a function of shield thickness on the Martian surface.

In Figure 4, the total dose equivalent and effective dose values computed on the surface are compared to half of the free space results. The free space results are computed using the ray-by-ray methodology described in section 2 without the presence of the atmosphere or Martian regolith. The factor of ½ is applied to the end result to approximately account for planetary blockage. The increase in free space and surface dose equivalent values beyond 45 g/cm^2 of aluminum does not continue indefinitely. The curves reach a maximum value just beyond 100 g/cm^2, and decline monotonically with increasing shield thickness. The exact location of the peak value within the Martian subsurface has been examined with Monte Carlo simulations for dose [Dartnell et al. 2007b, Morthekai et al. 2007], but not dose equivalent or effective dose. Nonetheless, in order to obtain any meaningful reduction in exposure, one would need to use shielding thicknesses much larger than where the peak value occurs, corresponding to several hundred g/cm^2 of shielding mass.

The comparison in Figure 4 is given to clarify that shielding optimization strategies will be different for deep space transit and surface operations. In free space, the exposure is reduced by about 45-65% for dose equivalent and 25-35% for effective dose over the first 20 g/cm^2 of shielding. In the case of aluminum, a clear minimum occurs in the dose equivalent-depth curve and a less pronounced minimum occurs in the effective dose-depth curve at about 45 g/cm^2. The variation of effective dose near the minimum value is within the transport code uncertainty as determined by comparisons with Monte Carlo simulations [Slaba et al. 2013]. It is therefore possible that the effective dose minimum is an artifact of transport code error, and the curve should actually continue to gradually decrease with depth. From a design standpoint, whether it is actually a minimum is less important than the fact there is no significant benefit from shielding after 45 g/cm^2 if the composition is similar to aluminum. This suggests a shielding strategy that would take advantage of the sudden drop due to thin amounts of shielding (< 20 g/cm^2) by distributing mass isotropically around the vehicle, as one might expect given the non-radiation related design constraints. After this initial stage of optimization, additional parasitic shielding mass could be added in specific regions to mitigate directional exposures.

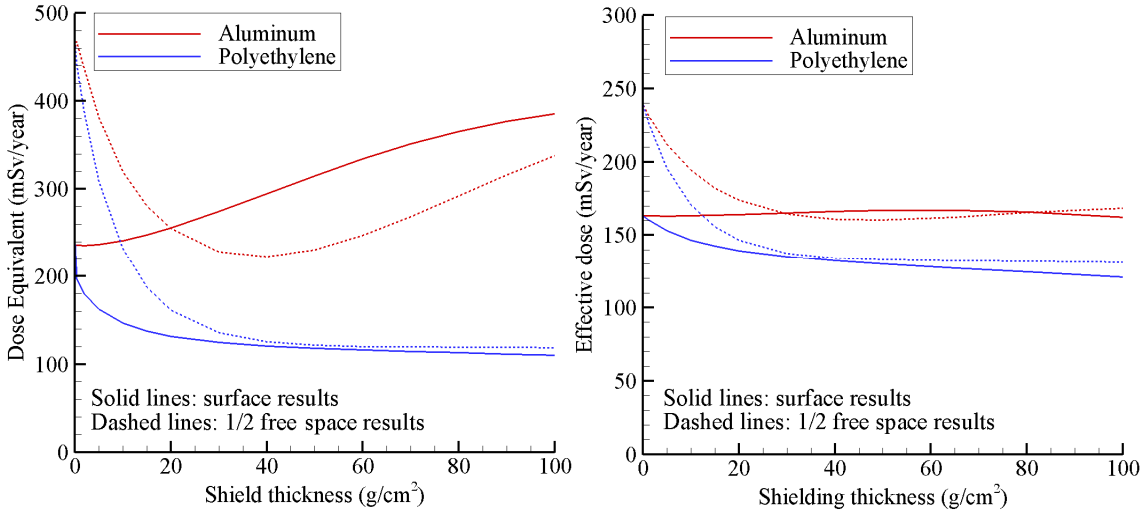

Figure 4. Comparison of surface exposure to ½ free space exposure as a function of shield thickness.

The surface results show that any reasonable amount of aluminum does not have a noticeable impact on effective dose, and consequently, adding or rearranging shielding mass on the surface will not appreciably reduce exposures. An in-situ shielding strategy will also be of little help unless several hundred g/cm^2 of regolith is utilized. Such a strategy would probably require large scale excavation making it an unlikely candidate. Instead, the shielding strategy would rely primarily on material optimization. Options, such as replacing aluminum structures with high hydrogen content carbon composites, could be pursued.

4. Summary and Conclusions

In this work, a computational model was described that allows exposures to be computed on the surface of Mars. The model utilizes the HZETRN-π/EM transport code in a ray-by-ray approach that includes the atmospheric cascade and secondary albedo neutrons. The model was found to be within 20% of a published Monte Carlo result; more comparisons are needed for further verification. Dose equivalent and effective dose values were computed as a function of aluminum and polyethylene shield thickness during solar minimum for surface and free space conditions. It was found that any reasonable amount of aluminum thickness increases dose equivalent and effective dose values on the surface. In the case of dose equivalent on the surface, the increase was quite dramatic (63%); in the case of effective dose on the surface, exposures varied by less than 3%. Both exposure quantities decrease monotonically with increasing polyethylene thickness. The marked difference between the materials is attributed mainly to the hydrogen content in the polyethylene.

The results shown in this work may be significant for vehicle optimization studies related to future Mars missions. In particular, the optimization strategy implemented for deep space transit will be able to take advantage of a reduction in exposure over the first 20-40 g/cm^2 of shielding. Though the shielding effectiveness of polyethylene is better than aluminum, both materials provide some exposure reduction over thicknesses typically found in transportation vehicles. A noticeable minimum in the exposure-depth curve near 45 g/cm^2 also helps constrain the optimization phase space. As discussed in section 3, whether the minimum is an artifact of transport code error or not, the response curve beyond 45 g/cm^2 is not likely to decline rapidly enough to justify the mass incurred with such large shielding thicknesses. Conversely, optimization strategies on the surface will not be able to take advantage of any exposure reduction from aluminum shielding, and in-situ shielding strategies will require prohibitively large shielding thicknesses (greater than several hundred g/cm^2) to provide any meaningful reduction. Material optimization strategies utilizing hydrogenated carbon composites could be pursued instead.

5. References

Blattnig, S. R., Norbury, J. W., Norman, R. B., Wilson, J. W., Singleterry, R. C., Tripathi, R. K., MESTRN: A Deterministic Meson-Muon Transport Code for Space Radiation. NASA Technical Memorandum 212995 (2004).

Borggrafe, A., Quatmann, M., Nolke, D., Radiation Protective Structures on the Base of a Case Study for a Manned Mars Mission. Acta Astronautica, Volume 65, pp. 1292-1305 (2009).

Clowdsley, M.S., Wilson, J.W., Kim, M.Y., Singleterry, R.C., Tripathi, R.K., Heinbockel, J.H., Badavi, F.F., Shinn, J.L., Neutron Environments on the Martian Surface. 11th Annual NASA Space Radiation Health Investigators' Workshop. Arona, Italy (2000).

Cucinotta, F.A., Hu, S., Schwadron, N.A., Kozarev, K., Townsend, L.W., Kim, M.Y., Space Radiation Risk Limits and Earth-Moon-Mars Environmental Models. Space Weather, Volume 8, S00E09 (2010).

Cucinotta, F.A., Kim, M.Y., Chappell, L.J., Evaluating Shielding Approaches to Reduce Space Radiation Cancer Risks. NASA Technical Memorandum 2012-217361 (2012).

Dartnell, L.R., Desorgher, L., Ward, J.M., Coates, A.J., Modeling the Surface and Subsurface Martian Radiation Environment: Implications for Astrobiology. Geophysical Research Letters, Volume 34, L02207 (2007a).

Dartnell, L.R., Desorgher, L., Ward, J.M., Coates, A.J., Martian Sub-Surface Ionizing Radiation: Biosignatures and Geology. Biogeosciences, Volume 4, pp. 545-558 (2007b).

De Angelis, G., Clowdsley, M.S., Singleterry, R.C., Wilson, J.W., A New Mars Radiation Environment Model with Visualization. Advances in Space Research, Volume 34, pp. 1328-1332 (2004).

ICRP, 1990 Recommendations of the International Commission on Radiological Protection. ICRP Publication 60, Pergamon (1990).

ICRP, 2007 Recommendation of the International Commission on Radiological Protection. ICRP Publication 103, Pergamon (2007).

Kim, M.Y., Thibeault, S.A., Simonsen, L.C., Wilson, J.W., Comparison of Martian Meteorites and Martian Regolith as Shield Materials for Galactic Cosmic Rays. NASA Technical Paper 1998-208724 (1998).

Kramer, R., Vieira, J.W., Khoury, H.J., Lima, F.R.A., Loureiro, E.C.M., Lima, V.J.M., Hoff, G., All about FAX: A Female Adult Voxel Phantom for Monte Carlo Calculations in Radiation Protection Dosimetry. Physics in Medicne and Biology, Volume 49, pp. 5203-5216 (2004).

Matthia, D., Berger, D., Mrigakshi, A.I., Reitz, G., A Ready-to-use Galactic Cosmic Ray Model. Advances in Space Research, Volume 51, pp. 329-338 (2013).

McKenna-Lawlor, S., Goncalves, P., Keating, A., Morgado, B., Heynderickx, D., Nieminen, P., Santin, G., Truscott, P., Lei, F., Foing, B., Balaz, J., Characterization of the Particle Radiation Environment at Three Potential Landing Sites on Mars using ESA's MEREM Models. Icarus, Volume 218, pp. 723-734 (2012a).

McKenna-Lawlor, S., Goncalves, P., Keating, A., Reitz, G., Matthia, D., Overview of Energetic Particle Hazards During Prospective Manned Missions to Mars. Planetary and Space Science, Volume 63, pp. 123-132 (2012b).

Millour, E., Forget, F., Lewis, S.R., Mars climate database v4.3 detailed design document, Le Laboratoire de M´et´eorologie Dynamique (2008). Available at http://www-mars.lmd.jussieu.fr/

Morthekai, P., Jain, M., Dartnell, L., Murray, A.S., Botter-Jensen, L., Desorgher, L., Modeling of the Dose-Rate Variations with Depth in the Martian Regolith using Geant4. Nuclear Instruments and Methods in Physics Research A, Volume 580, pp. 667-670 (2007).

NASA, Human Exploration of Mars Design Reference Architecture 5.0. NASA Special Publication 2009-566 (2009).

Norman, R. B., Blattnig, S.R., Angelis, G. D., Badavi, F.F., Norbury, J.W., Deterministic Pion and Muon Transport in Earth's Atmosphere. Advances in Space Research, Volume 50, pp. 146-155 (2012).

Norman, R.B., Slaba, T.C., Blattnig, S.R., An Extension of HZETRN for Cosmic Ray Initiated Electromagnetic Cascades. Advances in Space Research, in press (2013). Available at http://dx.doi.org/10.1016/j.asr.2013.01.021.

Nymmik, R.A., Panasyuk, M.I., Suslov, A.A., Galactic Cosmic Ray Flux Simulation and Prediction. Advances in Space Research, Volume 17, pp. 19-30 (1996).

O'Neill, P.M., Badhwar-O'Neill Galactic Cosmic Ray Flux Model – Revised. IEEE Transactions on Nuclear Science, Volume 57, pp. 3148-3153 (2010).

Saganti, P.B., Cucinotta, F.A., Wilson, J.W., Simonsen, L.C., Zeitlin, C., Radiation Climate Map for Analyzing Risks to Astronauts on the Mars Surface from Galactic Cosmic Rays. Space Science Review, Volume 110, pp. 143-156 (2004).

Simonsen, L.C., Nealy, J.E., Townsend, L.W., Wilson, J.W., Radiation Exposure for Manned Mars Missions. NASA Technical Paper 2979 (1990).

Simonsen, L.C. and Nealy, J.E., Radiation Protection for Human Missions to the Moon and Mars. NASA Technical Paper 3079 (1991).

Slaba, T.C., Blattnig, S.R., Aghara, S.K., Townsend, L.W., Handler, T., Gabriel, T.A., Pinsky, L.S., Reddell, B., Coupled Neutron Transport for HZETRN. Radiation Measurements, Volume 45, pp. 173-182 (2010a).

Slaba, T.C., Blattnig, S.R., Badavi, F.F., Faster and more Accurate Transport Procedures for HZETRN. Journal of Computational Physics, Volume 229, pp. 9397-9417 (2010b).

Slaba, T.C., Qualls, G.D., Clowdsley, M.S., Blattnig, S.R., Walker, S.A., Simonsen, L.C., Utilization of CAM, CAF, MAX, and FAX for Space Radiation Analyses using HZETRN. Advances in Space Research, Volume 45 pp. 866-883 (2010c).

Slaba, T.C., Blattnig, S.R., Clowdsley, M.S., Variations in Lunar Neutron Dose Estimates. Radiation Research, Volume 176, pp. 827-841 (2011).

Slaba, T.C., Blattnig, S.R., Reddell, B., Bahadori, A., Norman, R.B., Badavi, F.F., Pion and Electromagnetic Contribution to Dose: Comparisons of HZETRN to Monte Carlo Results and ISS Data. Advances in Space Research, accepted for publication (2013).

SPENVIS, available at http://spenvis.oma.be/

Wilson, J.W., Townsend, L.W., Schimmerling, W., Khandelwal, G.S., Khan, F., Nealy, J.E., Cucinotta, F.A., Simonsen, L.C., Shinn, J.L., Norbury, J.W., Transport Methods and Interactions for Space Radiations. NASA Reference Publication 1257 (1991).

Wilson, J.W., Miller, J., Konradi, A., Cucinotta, F.A., eds. Shielding Strategies for Human Space Exploration. NASA Conference Publication 3360 (1997).

Wilson, J.W., Clowdsley, M.S., Cucinotta, F.A., Tripathi, R.K., Nealy, J.E., De Angelis, G., Deep Space Environments for Human Exploration. Advances in Space Research, Volume 34, pp. 1281-1287 (2004).

Wilson, J.W., Tripathi, R.K., Badavi, F.F., Cucinotta, F.A., Standardized Radiation Shield Design Method: 2005 HZETRN. Society of Automotive Engineers International Conference on Environmental Systems, 2006-18 (2006).

Zeitlin, C., Cleghorn, T., Cucinotta, F., Saganti, F., Anderson, V., Lee, K., Pinsky, L., Atwell, W., Turner, R., Badhwar, G., Overview of the Martian Radiation Environment Experiment. Advances in Space Research, Volume 33, pp. 2204-2210 (2004).

REPORT DOCUMENTATION PAGE

Form Approved
OMB No. 0704-0188

1. REPORT DATE *(DD-MM-YYYY)*	2. REPORT TYPE	3. DATES COVERED *(From - To)*
01- 04 - 2013	Technical Publication	

4. TITLE AND SUBTITLE

Radiation Shielding Optimization on Mars

5a. CONTRACT NUMBER

5b. GRANT NUMBER

5c. PROGRAM ELEMENT NUMBER

6. AUTHOR(S)

Slaba, Tony C.; Mertens, Christopher J.; Blattnig, Steve R.

5d. PROJECT NUMBER

5e. TASK NUMBER

5f. WORK UNIT NUMBER

651549.02.07.10

7. PERFORMING ORGANIZATION NAME(S) AND ADDRESS(ES)

NASA Langley Research Center
Hampton, VA 23681-2199

8. PERFORMING ORGANIZATION REPORT NUMBER

L-20242

9. SPONSORING/MONITORING AGENCY NAME(S) AND ADDRESS(ES)

National Aeronautics and Space Administration
Washington, DC 20546-0001

10. SPONSOR/MONITOR'S ACRONYM(S)

NASA

11. SPONSOR/MONITOR'S REPORT NUMBER(S)

NASA/TP-2013-217983

12. DISTRIBUTION/AVAILABILITY STATEMENT

Unclassified - Unlimited
Subject Category 93
Availability: NASA CASI (443) 757-5802

13. SUPPLEMENTARY NOTES

14. ABSTRACT

Future space missions to Mars will require radiation shielding to be optimized for deep space transit and an extended stay on the surface. In deep space, increased shielding levels and material optimization will reduce the exposure from most solar particle events (SPE) but are less effective at shielding against galactic cosmic rays (GCR). On the surface, the shielding provided by the Martian atmosphere greatly reduces the exposure from most SPE, and long-term GCR exposure is a primary concern. Previous work has shown that in deep space, additional shielding of common materials such as aluminum or polyethylene does not significantly reduce the GCR exposure. In this work, it is shown that on the Martian surface, almost any amount of aluminum shielding increases exposure levels for humans. The increased exposure levels are attributed to neutron production in the shield and Martian regolith as well as the electromagnetic cascade induced in the Martian atmosphere. This result is significant for optimization of vehicle and shield designs intended for the surface of Mars.

15. SUBJECT TERMS

Deep space; HZETRN; Mars radiation; Risk; Space radiation

16. SECURITY CLASSIFICATION OF:			17. LIMITATION OF ABSTRACT	18. NUMBER OF PAGES	19a. NAME OF RESPONSIBLE PERSON
a. REPORT	b. ABSTRACT	c. THIS PAGE			STI Help Desk (email: help@sti.nasa.gov)
					19b. TELEPHONE NUMBER *(Include area code)*
U	U	U	UU	17	(443) 757-5802